JACS Au
AN OPEN ACCESS JOURNAL OF THE AMERICAN CHEMICAL SOCIETY

pubs.acs.org/jacsau

Article

Scalable Formation of Diamine-Appended Metal–Organic Framework Hollow Fiber Sorbents for Postcombustion CO_2 Capture

Wenying Quan, Hannah E. Holmes, Fengyi Zhang, Breanne L. Hamlett, M. G. Finn, Carter W. Abney, Matthew T. Kapelewski, Simon C. Weston,* Ryan P. Lively,* and William J. Koros*

Cite This: *JACS Au* 2022, 2, 1350–1358

Read Online

ACCESS | Metrics & More | Article Recommendations | Supporting Information

ABSTRACT: We describe a straightforward and scalable fabrication of diamine-appended metal–organic framework (MOF)/polymer composite hollow fiber sorbent modules for CO_2 capture from dilute streams, such as flue gas from natural gas combined cycle (NGCC) power plants. A specific Mg-MOF, Mg_2(dobpdc) (dobpdc^{4-} = 4,4′-dioxidobiphenyl-3,3′-dicarboxylate), incorporated into poly(ether sulfone) (PES) is directly spun through a conventional "dry-jet, wet-quench" method. After phase separation, a cyclic diamine 2-(aminomethyl)piperidine (2-ampd) is infused into the MOF within the polymer matrix during postspinning solvent exchange. The MOF hollow fibers from direct spinning contain as high as 70% MOF in the total fibers with 98% of the pure MOF uptake. The resulting fibers exhibit a step isotherm and a "shock-wave-shock" breakthrough profile consistent with pure 2-ampd-Mg_2(dobpdc). This work demonstrates a practical method for fabricating 2-ampd-Mg_2(dobpdc) fiber sorbents that display the MOF's high CO_2 adsorption capacity while lowering the pressure drop during operation.

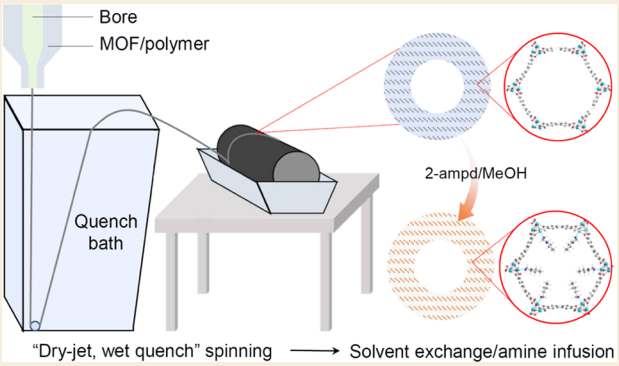

KEYWORDS: *CO_2 capture, hollow fiber sorbent, metal–organic framework, step adsorption, amine functionalization*

INTRODUCTION

Global energy-related carbon dioxide emissions, which now account for about 65% of all anthropogenic greenhouse gas emissions, have risen from approximately 20 Gt in 1990 to 31.5 Gt in 2020 contributing to CO_2 reaching its highest-ever average annual concentration in the atmosphere of 412.5 ppm.[1,2] The capture of CO_2 from flue gases using technologies such as absorption, adsorption, and membranes can mitigate this trend. Aqueous amine absorption (amine scrubbing), while effective,[3] requires high energy consumption and must contend with corrosion and degradation issues. The regeneration energy for CO_2 absorption is from 3.24 to 4.2 GJ/tonne CO_2[4] due to the strong affinity between CO_2 and amines and the high heat capacity of the solvent, while the regeneration energy for adsorption lies between 1.9 and 3.23 GJ/tonne CO_2 depending on the adsorbent and cyclic process.[5−8] Adsorption also benefits from mild regeneration conditions, desirable adsorption kinetics, absence of corrosive chemicals, and good long-term stability. However, improvements in adsorbent media, contactors, and process designs are necessary to ensure economic feasibility in replacing the existing absorptive technology; viability will rely not only on lowering energy demands but also on reducing the capital cost.

Diverse materials have been investigated for adsorption-based CO_2 capture systems, including silicas, carbons, zeolites, metal oxides, and metal–organic frameworks (MOFs).[3,4,9−12] MOFs offer high surface areas and pore volumes, tailorability (e.g., diverse metal species, difference in organic linkers, installation of various functional groups), chemical versatility, and good thermal stability. For these reasons, MOFs have been highly studied for CO_2 capture applications at the laboratory scale; however, the economics of the MOF scale-up remains a largely unanswered question. Functionalizing MOF metal sites with amines has recently been developed as a method to further improve adsorption performance and to engineer the shape of the adsorption isotherm, enabling energy-efficient cyclic adsorption processes.[13,14] Choi et al.[15] functionalized Mg_2(dobdc) (dobdc = 2,5-dioxido-1,4-benzenedicarboxylate) with ethylenediamine (ED) to achieve a stable capacity of approximately 1.51 mmol CO_2/g-sorb from an ultradilute CO_2 gas stream (400 ppm CO_2). The expanded framework, M_2(dobpdc) (M = Zn, Mg, Fe, Co, Mn; dobpdc = 4,4′ = dioxidobiphenyl-3,3′-dicarboxylate), enables amine functionalization on the open metal sites to further improve CO_2 adsorption.[16,17] After grafting diamines, adsorption on such

Received: January 15, 2022
Revised: April 20, 2022
Accepted: April 20, 2022
Published: May 16, 2022

https://doi.org/10.1021/jacsau.2c00029
JACS Au 2022, 2, 1350–1358

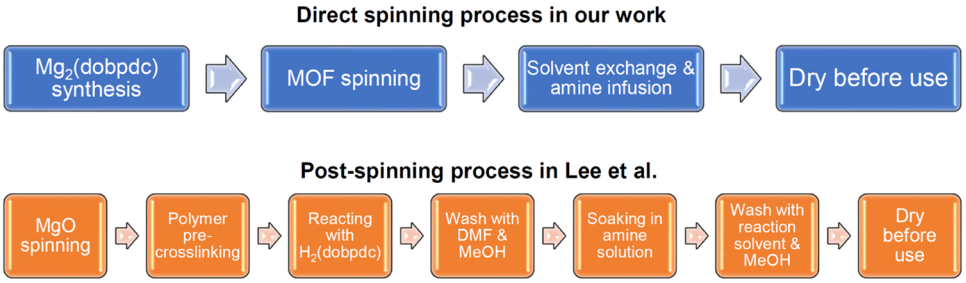

Figure 1. Flow charts comparing direct spinning in this work and the postspinning process.[32]

MOFs exhibits a step adsorption isotherm,[16−18] which increases the working capacity with smaller temperature swings compared to a classic type I isotherm on open metal site MOFs from 3.3 to 4.1 mol CO_2/g-MOF within a temperature swing range of 140−35 °C. A specific cyclic 1°/2° diamine, 2-(aminomethyl)piperidine (2-ampd),[18] was appended to metal sites in Mg_2(dobpdc) (chemical structure is shown in Figure S1) with good thermal stability and full chemisorption capacity of CO_2 at low pressures. Through modification of steric interactions of 2-ampd, a unique step adsorption isotherm was observed. Moreover, CO_2 adsorption was greatly improved under humid conditions. Due to the benefits of such 2-ampd-Mg_2(dobpdc), this diamine-appended MOF is ideal for incorporating into hollow fibers for CO_2 capture from the natural gas combined cycle (NGCC) through temperature swing adsorption (TSA) processes.

Despite such progress in terms of adsorption media, conventional adsorption contactors still highly rely on packed adsorbent beds with solid particles or expensive monolith contactors. Pellet-based systems suffer from high pressure drops and extended mass transfer zones, resulting in inefficient adsorbent utilization. Moreover, in the special case of 2-ampd-appended-Mg_2(dobpdc), the nonisothermal operation typically associated with packed beds increases the cost of the separation process.[19] Indeed, active thermal management (i.e., cooling during adsorption) has been identified as a critical aspect in the development of sorbents with type V isotherms.[19] To develop amine-functionalized MOFs for future implementation and commercialization, an alternative approach is needed. Koros, Lively, and co-workers[20−26] previously developed hollow fiber sorbents for rapid cyclic adsorption/desorption processes, which allow for localized thermal management via flowing water in the fiber bore. Hollow fiber sorbents also provide low pressure drop, shorten the mass transfer zone, and enable a rapid temperature swing (i.e., CO_2 adsorption/desorption cycle of < 4 min) along with possible effective heat integration if a water-resistant layer is installed on the bore side.

First-generation sorbents used zeolites blended with cellulose acetate (CA) in the fiber wall,[20] and later, polyethylenimine (PEI)-infused silica- and amine-grafted silica hollow fiber sorbents were used for improved CO_2 sorption capacities under humid conditions.[22−25,27] Typically, the preparation of hollow fiber sorbents relies on the use of polar solvents to give uniform sorbent dispersion via sonication, which is ultimately followed by a water quench in the spinning process. These harsh conditions often induce a variety of MOF degradation problems. So far, only MIL-101(Cr)[28] and UiO-66[28,29] have been reported to survive such a spinning procedure while maintaining nearly 90% of the MOF-based capacities. Formation of monoliths/hollow fibers with several water-sensitive MOFs[30−32] was reported using postspinning growth of MOF crystals onto and into precursor monoliths and hollow fibers, respectively. Among this class of fiber sorbents, a Mg_2(dobpdc) hollow fiber sorbent was also reported and prepared through multistep pre-cross-linking of polymer supports and post-treatment of a precursor (MgO) hollow fiber. As shown in the flow chart of the postspinning process in Figure 1, the complexity of this approach will complicate scale-up, suggesting that more streamlined methods are needed.[32]

To enable scalable preparation of a Mg_2(dobpdc)/2-ampd-Mg_2(dobpdc) hollow fibers, the present work aims to develop a simplified protocol for incorporating such MOFs into polymeric fibers for utilization in carbon capture systems. Thus, a direct spinning process is proposed as shown in the flow chart in Figure 1, simplifying the preparation process. Our preliminary work on the stability of Mg_2(dobpdc) under real fiber spinning conditions (Figure S2) is the first evidence of directly spinning an open metal site MOF, in contrast to previous studies that have either utilized MOFs without open metal sites or complex postspinning MOF crystal growth methods. In particular, we explored the feasibility of incorporating 2-ampd-Mg_2(dobpdc) into conventional commercially available polymers [i.e., cellulose acetate (CA), polyimides (Matrimid and Torlon), and poly(ether sulfone) (PES)] and novel, synthesized polymers [polymer of intrinsic microporosity (PIM-1) and amidoximized PIM-1 (AO-PIM-1)]. We also optimized the MOF loading amount and studied the effects of pore formers and spinning conditions. After extrusion and phase separation, the hollow fibers went through methanol exchange followed by diamine postinfusion in methanol. These fibers were used in dynamic breakthrough experiments with simulated NGCC dry flue gas (4.5% CO_2) to demonstrate the sorption performance of these materials.

MATERIALS AND METHODS

Materials

$Mn_{0.12}Mg_{1.88}$(dobpdc) was prepared as published previously.[33,34] 2-(aminomethyl)piperidine (2-ampd) for diamine grafting was purchased from Sigma-Aldrich.

Commercially available polymers were used as polymer supports for the MOF and are listed in Table S1. These polymers include cellulose acetate (CA) (M_w = 50,000, Sigma-Aldrich), poly(amide-imide) (PAI, Torlon, Solvay Advanced Polymers), polyimide Matrimid 5218 (Huntsman International LLC), and poly(ether sulfone) (PES, Veradel 3000P, Solvay). Both lithium nitrate ($LiNO_3$, ReagentPlus) and poly(vinylpyrrolidone) (PVP, M_w = 55,000) were purchased from Sigma-Aldrich for use as pore formers.

In addition, novel polymers, polymer of intrinsic microporosity (PIM-1) and amidoximized PIM-1 (AO-PIM-1), were studied as supports for 2-ampd-Mg_2(dobpdc). The synthesis of PIM-1 followed the low-temperature process described in Jue et al.'s work.[35,36] The

https://doi.org/10.1021/jacsau.2c00029
JACS Au 2022, 2, 1350−1358

modification of amidoxime on PIM-1 used the same procedure as our previous work,[37] and detailed procedures for synthesizing PIM-1 and AO-PIM-1 are shown in the Supporting Information.

The solvents in the polymer dope solutions are tetrahydrofuran (THF) (anhydrous, with 250 ppm BHT as an inhibitor, >99%, from Sigma-Aldrich) for PIM-1 and *N*-methyl-2-pyrrolidone (NMP) (ReagentPlus 99%, Sigma-Aldrich, Milwaukee) for other polymers. The nonsolvent for PIM-1 is *N*,*N*-dimethylacetamide (DMAc) (anhydrous, 98.5%, Sigma-Aldrich), while deionized water (H_2O) was used for other polymers. Methanol (99.8%, ACS Reagent, Sigma-Aldrich) and hexanes (ACS Reagent, 98.5%, Baker) were used as solvent exchange agents. Lithium nitrate ($LiNO_3$) (ReagentPlus, Sigma-Aldrich) was used as an alternate pore former instead of PVP, as will be explained below.

Some of the chemicals for PIM-1 synthesis were purchased from Fisher Scientific including tetrafluoroterephthalonitrile (TFTPN) (98%), 5,5′,6,6′-tetrahydroxy-3,3,3′,3′,-tetramethyl-1,1′,-spirobisindane (TTSBI) (Alfa Aesar, 97%), and potassium carbonate (K_2CO_3) (Alfa Aesar, anhydrous, 99%). The solvent for the synthesis was *N*,*N*-dimethylformamide (DMF, anhydrous, 99.8%), purchased from Sigma-Aldrich. Ultrahigh purity (UHP, >99.99%) gases were purchased from Airgas.

Fiber Contactor Formation

A range of dope solutions were prepared for syringe extrusion to optimize dope properties in 20 mL vials, and the compositions of each polymer dope are listed in Table S2. Polymer dopes were prepared and mixed homogeneously on a heated roller at about 50−60 °C. Afterward, the desired amount of MOF particles was added and blended into the polymer dope. The mixture was sonicated three times for 30 s each with a 1 min interval to avoid the collapse of MOF crystals. The sonication horn is a VCX130 model from Sonics & Materials Inc. with a maximum power output of 130 watts and a frequency of 20 kHz. After extruding by syringe, the fibers were set in a quench bath for complete phase separation, followed by solvent exchange by methanol and hexane. Then, the fibers were dried in a vacuum oven overnight at 60 °C.

A conventional "dry-jet, wet-quench" spinning method was used for fiber formation. In addition, a third pump with solvent-only solutions was used to remove undesired skin layers. The schematic figure and spinning conditions are shown in Figure S3 and Table S3.

After extrusion, the fibers were placed in deionized water for 3 days for complete solvent removal, with the water being replaced once a day; this process is faster in industrial settings due to roll-to-roll processing capability. Afterward, the fibers underwent a solvent exchange process with methanol three times for 20 min each time. Prior to solvent exchange with hexane, the fibers were immersed in a 5 vol % 2-ampd/MeOH solution overnight for diamine postinfusion. The fibers were transferred from the methanol bath to a fume hood to air dry for about 1 h and then dried in a vacuum oven overnight at 50 °C.

Fiber Sorbent Characterizations

CO_2 sorption performance was tested via a thermogravimetric analyzer (TGA; TA Instruments SDT Q50). The adsorption program and time−temperature profile are shown in Figure S4. For adsorption kinetic analysis (Figure S4a), a pure CO_2 gas flow was introduced into the sample chamber with a 23 sccm flow rate at 25 °C after pretreatment with 37 sccm N_2 at 110 °C for 240 min. The CO_2 adsorption isobar was obtained using 23 sccm CO_2 (using N_2 as a balance gas) with a 1 °C/min ramp rate from 140 to 35 °C at 1 atm, as shown in Figure S4b.

CO_2 adsorption isotherms at different temperatures were measured on a Micromeritics ASAP 2020 instrument. Prior to isotherm measurements, the fibers were regenerated under 100 sccm of Ar at 120 °C for 1 h, followed by 4 h at <10 μbar at 100 °C. Lower pressure data points (<6 mmHg) were allowed to equilibrate for 1.5 h, while higher pressure data points (>6 mmHg) were considered equilibrated after <0.01% change over 30 s intervals.

The framework structures before and after treatment in the major spinning conditions were analyzed by X-ray diffraction (XRD) using an Empyrean XRD system from PANalytical. The ramp rate was 3°/min within a range of 2−60°.

Scanning electron microscopy (SEM) was performed for MOF morphologies before and after hollow fiber incorporation by a Hitachi SU8230 SEM instrument. For the morphology of hollow fiber sorbents, a Hummer 6 gold/palladium sputter coater was used for sputter-coating with gold to less than 20 nm thickness before SEM analysis.

A Thermo Scientific iSO50 ATR spectrophotometer was used for attenuated total reflectance-Fourier transform infrared (ATR-FTIR) analysis. The spectra were recorded by the KBr technique within a range of 4000−650 cm^{-1}.

^1H NMR spectra on MOF powders treated with different solvents were obtained from a Bruker Advance IIIHD 500 instrument. Before analysis, MOF powder was suspended in 1−2 mL of fresh DMSO-d_6. Afterward, one to two drops of DCl in D_2O was added into the suspension, which could be dissolved completely by heating and sonication.

Permeance Tests

To characterize pore network interconnectivity, pure gas permeances of the hollow fiber sorbent were tested after assembling the module, as shown in Figure S5. The module was kept in a permeation box at 35 °C and connected to the feed gas through the shell side at 15, 30, or 100 psig. The flow rate of the permeated gas from the bore side was measured by a bubble flow meter, and the permeance was calculated by eq 1. The results from the average of three modules were used in each case.

$$\frac{P}{l_f} = \frac{Q_{perm}}{\pi d_f L_{perm}(p_{feed} - p_{perm})} \quad (1)$$

Note that P/l_f is the gas permeance, which is the pressure-normalized gas flux; Q_{perm} is the flow rate of the permeate; d_f is the fiber outer diameter, while L_{perm} is the fiber's effective length; and p_{feed} and p_{perm} are pressures of the feed gas and permeate gas, respectively. The permeance unit is GPU as described in eq 2.

$$1\ \text{GPU} = 1 \times 10^{-6} \frac{\text{cm}^3(\text{STP})}{\text{cm}^2 \times \text{s} \times \text{cmHg}} \quad (2)$$

Helium (He), nitrogen (N_2), oxygen (O_2), and carbon dioxide (CO_2) permeances were tested under 35 °C and 100 psig.

Breakthrough Tests

A 38.74 cm long stainless-steel tube (0.95 cm OD with 0.09 cm wall thickness) was packed with 4.1 g of fibers (24 fibers with approx. 68 wt % 2-ampd-Mg_2(dobpdc) in total). The fiber module was wrapped in heat tape and activated at 120 °C under 139 sccm argon flow for 18 h before the first breakthrough and regenerated under the same conditions for 4 h between subsequent breakthroughs. The desorption times were extended significantly past what was required as an extra precaution. Figure S6 shows a near-zero CO_2 concentration after approximately 15 min under these desorption conditions. At the end of regeneration, the mass spectrometer (MS) inlet was opened, and the outlet gas was scanned to ensure full regeneration (no H_2O or CO_2 signal). The heat was adjusted to the analysis temperature (40 or 50 °C) and the module was allowed to cool under argon flow. The flue gas mixture containing 4.5% CO_2 and 4.5% He balanced with N_2 was directed to the MS in a bypass line and scanned to ensure the lines were clean (only CO_2, He, N_2). The flue gas was then directed through the bed with the following m/z ratios measured: 4 (He), 14 (N_2), 18 (H_2O), 20 (Ar), 40 (Ar), and 44 (CO_2).

The CO_2 and He concentrations as a function of time were used to find the adsorbent capacity. Helium was used as a tracer to account for the dead volume in the system. The C/C_0 value for each was determined by dividing $C(t)$ by C_0 (feed concentration). Equation 3 was then used to find the adsorption capacity,

https://doi.org/10.1021/jacsau.2c00029
JACS Au 2022, 2, 1350−1358

$$q_{CO_2} = \frac{Q \cdot C_{0,CO_2}}{m_s} \int_0^{t_s} \left(\frac{C_{He}(t)}{C_{0,He}} - \frac{C_{CO_2}(t)}{C_{0,CO_2}} \right) [s]\, dt \quad (3)$$

where q_{CO_2} is the adsorption capacity [mol/g], Q is the total gas flow rate [mol/s], C_{0,CO_2} is the feed CO_2 concentration [mol CO_2/total mol], $C_{0,He}$ is the feed helium concentration [mol He/total mol], and m_s is the mass of the sorbent in the bed [g].

RESULTS AND DISCUSSION

Mg_2(dobpdc) Hollow Fiber Sorbent Spinning

In our preliminary work on polymer selection, the MOF was preserved regardless of which polymer support was used (shown in Supporting Information, Figure S7). CO_2 adsorption kinetic performance shown in Figure S8 on different polymer-supported 2-ampd-Mg_2(dobpdc) samples were different due to their intrinsic diffusion coefficient, skin layer formation, and pore structure after phase separation. The final CO_2 uptake of the fiber (Figure S9) was not only contributed by the MOF but also by the polymer networks, as some of the polymers are capable of adsorbing CO_2. Among the tested polymer networks, PES was found to have the best performance as it exhibits good thermal stability (Figure S10) and fast adsorption kinetics due to the open pore structure, as shown in Figure S11. CA and AO-PIM-1 can also perform as polymer supports; however, the pore structures of both polymers are denser than PES, leading to transport resistance, as shown in Figure S11. Moreover, the MOF/CA hollow fiber forms a skin layer, which requires a third solvent pump during spinning to prevent the formation of this skin (Figure S12 and Table S3). PIM-1 was difficult to blend with the MOF homogeneously as a result of the usage of a highly volatile solvent (i.e., tetrahydrofuran, one of the few "spinnable" solvents for PIM-1) in the dope solution. Polyimide-based polymers, Matrimid and Torlon, on the contrary, were unable to support 2-ampd-Mg_2(dobpdc), which was tentatively attributed to the degradation of imides via amine exposure. Thus, PES-supported 2-ampd-Mg_2(dobpdc) hollow fibers were directly spun through a conventional "dry-jet, wet-quench" spinning process, as shown in Figure S3.

To spin MOF/PES, a PES dope with $LiNO_3$ was prepared for blending with 20 and 60 wt % Mg_2(dobpdc). Detailed dope compositions and spinning conditions are listed in Table S4. The cross section of the MOF hollow fiber can be seen in Figure 2a, revealing MOF crystals residing in the PES matrix, and a defective skin layer is also shown in Figure 2. As observed in the SEM images, no obvious skin layer was formed, in contrast to the CA-based hollow fibers shown in Figure S12. Pure gas permeances of Mg_2(dobpdc)/PES hollow fibers are shown in Table 1. These permeances are much higher than those of Mg_2(dobpdc)/CA hollow fibers (Table S8, Supporting Information). CO_2 permeance at 30 psi of 20 wt % Mg_2(dobpdc)/PES hollow fibers was 168,000 GPU, which was approximately 10 times higher than that of 20 wt % Mg_2(dobpdc)/CA hollow fibers, promoting much faster CO_2 adsorption. Such high gas permeances can be attributed to the open pore structure (as shown in Figure 2b) as well as percolating defects through the outer layer of the PES matrix (Figure 2d), which indicates that the polymer network barely hinders the CO_2 adsorption on MOF in hollow fibers. When the MOF loading increased to 60 wt %, gas permeance was further improved to 161,400 GPU at 15 psi. Additionally, compared with the gas permeance in other works on hollow fiber sorbents, N_2 permeance through MOF/PES is much higher than that through other hollow fiber sorbents, as listed in Table S8.

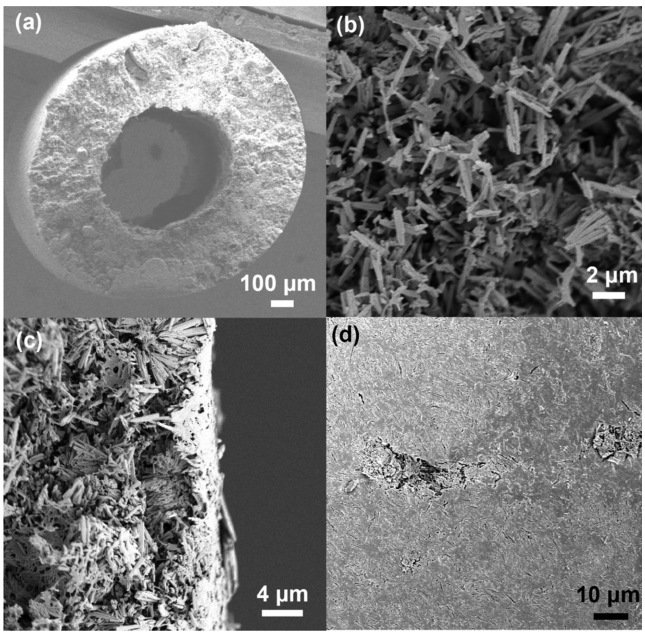

Figure 2. SEM images of 2-ampd-Mg_2(dobpdc)/PES hollow fibers. (a) Cross section of a 60 wt % Mg_2(dobpdc)/PES hollow fiber, (b) 60 wt % Mg_2(dobpdc) in a PES polymer matrix, (c) skin layer of a 60 wt % Mg_2(dobpdc)/PES hollow fiber, and (d) macroscopic defects on the outer skin layer.

Post-Spinning Infusion of 2-ampd on Mg_2(dobpdc)/PES Hollow Fiber Sorbents

Initial attempts at fiber spinning used MOFs that had already been appended with 2-ampd. While the framework of Mg_2(dobpdc) survived spinning conditions (Figure S2), we observed that the diamines were partially stripped away due to the strong affinity between amines and polar solvents (i.e., water in phase separation and methanol in solvent exchange). The loss is shown by a loss of the step in the CO_2 isobar (Figure S13) and a loss of proton signals in ^{1}H NMR tests (Figure S14). Due to the steric hindrance of 2-ampd in the framework, the CO_2 isobar on 2-ampd-Mg_2(dobpdc) has a rare two-step adsorption profile upon decreasing the adsorption temperature.[18] While Mg_2(dobpdc)/polymer composite contactors retain some CO_2 adsorption capacities (on open metal sites through type I adsorption, as in Table S5), the bare MOF tends to degrade gradually in air or flue gas when it associates with preadsorbed polar solvent molecules.[38,39] Thus, to preserve the stability of the MOF and enable the desired step CO_2 adsorption behavior, a procedure for appending diamines to the MOF in polymer contactors was necessary.

Considering this, we developed a scalable method for appending diamines on the MOF within a polymer network for hollow fiber sorbents.[40] In a typical fiber formation procedure, the hollow fibers are soaked in MeOH and hexane after completing phase separation in H_2O. The solvent exchange process minimizes pore collapse. However, the standard procedure for grafting 2-ampd onto Mg_2(dobpdc) uses toluene as a carrier solvent,[18] which is an undesired solvent during the spinning process due to its swelling effect on most polymers.[41] However, MeOH is a good solvent and carrier for amine chemicals into porous materials via capillary action. Labreche

https://doi.org/10.1021/jacsau.2c00029
JACS Au 2022, 2, 1350−1358

Table 1. Pure Gas Permeances of MOF Hollow Fibers Formed from Different Spinning Processes[a]

Mg_2(dobpdc) loading (wt %)	feed pressure (psi)	permeance (GPU)		
		N_2	CH_4	CO_2
20	30	205,000 ± 3600	266,000 ± 1500	168,000 ± 4800
60	15	169,600 ± 6800	220,000 ± 20,100	161,400 ± 4300

[a]Gas permeances were tested at 35 °C.

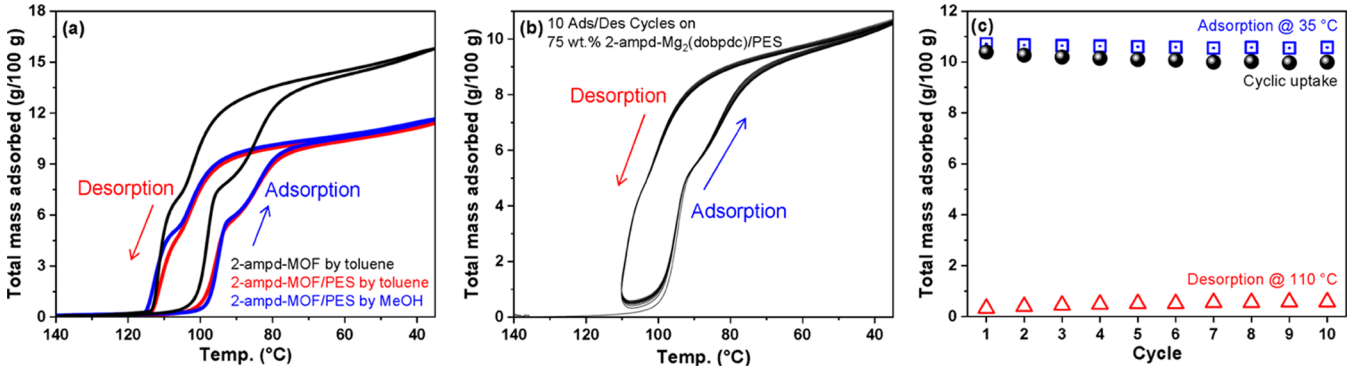

Figure 3. Adsorption isobars and regeneration test on 2-ampd-Mg_2(dobpdc)/PES fibers from syringe extrusion. (a) Two-step adsorption on 2-ampd-Mg_2(dobpdc)/PES fiber sorbents infused with different solvents (per 100 g of total fiber), (b) 10 adsorption/desorption cycles overlap on 2-ampd-Mg_2(dobpdc)/PES fiber sorbents, and (c) CO_2 uptake at 35 °C and desorption at 110 °C as well as the cyclic uptake.

et al.[22,25] introduced polyethylenimine (PEI) into porous materials/polymer hollow fiber sorbents by dissolving it in MeOH, and the resultant sorbents showed improved CO_2 adsorption performance. Inspired by that work, we used MeOH instead of toluene as an infusion medium to carry 2-ampd through the porous polymer, and the infused-diamines were grafted to the open metal sites in the MOF. Figure 3a compares CO_2 isobars of MOF/PES fiber sorbents for which MeOH and toluene were used as solvents for infusion. The two-step adsorption is evident for both 2-ampd/toluene and 2-ampd/MeOH infusion procedures, and both are consistent with that of pure 2-ampd-Mg_2(dobpdc).[18] Moreover, the fiber sorbent infused in 2-ampd/MeOH shows steeper, more discernible adsorption steps than that in 2-ampd/toluene, which can be ascribed to toluene-induced deformation of the PES pore structure. Furthermore, the final uptake at 35 °C on the fiber sorbent is about 11.62 g/100 g, which is approximately 73.5% of that on the pure MOF (i.e., 15.81 g/100 g). This result is consistent with the MOF loading in a mixed matrix dope before spinning (i.e., 75 wt % MOF in total fiber), indicating that 98% of the MOFs in the fiber are utilized for CO_2 capture. The difference in the final uptake of the MOF at 35 °C between this work and Siegelman et al.'s work[18] is ascribed to the different batches of MOFs from different sources. Thus, if a batch of MOF with higher sorption capacity is prepared, the fiber will achieve a higher CO_2 uptake. Of note, the initial adsorption step temperature of 100 °C is slightly lower than the step temperature of pure MOF samples. Such a shift in temperature can be associated with the thermal moderating effect caused by polymer networks. Another explanation may be due to mass transfer resistance ascribed to the porosity and the formed skin layer. In addition, residual solvent in the MOF may also contribute to the temperature shift.

Since the porous structure of the polymer network can also support diamines,[40] whether the diamines intermix with the polymer network or successfully append on metal sites is of great interest and deserves further investigation. For this purpose, CO_2 isobars on the pure PES fiber and MOF/PES fiber, prepared and infused in 2-ampd/MeOH, are compared in Figure S15. The pure PES infused with diamines were found to be incapable of adsorbing CO_2 at any appreciable level, demonstrating that the high levels of CO_2 uptake in the amine-appended MOF/PES fibers are a result of amine−MOF interactions. In addition to the CO_2 adsorption performance, we also observed translucent substance on the surface of 2-ampd/PES fibers after CO_2 exposure (Figure S15b,c), indicating that 2-ampd was physically packed in the pores of PES fibers. We also utilized a cyclic temperature swing test to provide evidence that the diamines are appended to metal sites within the MOFs. If diamines intermix with the polymer network, the diamines could be easily swept away through adsorption/desorption cycles due to the weak interaction between diamines and the polymer, ultimately leading to a drop in CO_2 uptake. Figure 3b shows the overlapping results of 10 adsorption/desorption cycles of the cyclic temperature swing test from 110 to 35 °C. The two-step adsorption occurs within all tested cycles, demonstrating the stable appending of diamine on the MOF inside the polymer network, as the amine polymer by itself is unable to afford a stepped isotherm or isobar. Furthermore, as shown in Figure 3c, the cyclic CO_2 uptake changes little, stabilizing at 2.2 mmol CO_2/g-fiber and 2.7 mmol CO_2/g-MOF. The value slightly lower than the theoretical value (i.e., 2.8 mmol CO_2/g-fiber) presumably reflects the inadequate adsorption time of the isobar adsorption technique; the value at equilibrium coincides with the 75 wt % uptake, as shown in Figure S16. Additionally, the CO_2 uptake can also be improved by optimizing the infusion conditions, which will be discussed in our future work.

To verify the versatility of this postinfusion approach, various amines were infused onto Mg_2(dobpdc)/PES. As shown in Figure S17, the isobars of these as-prepared adsorbents are analogous to those of the corresponding pure amine-appended MOFs. Therefore, the developed postinfusion approach is applicable to various diamine or triamine/MOF combinations, not only endowing them with chemical

https://doi.org/10.1021/jacsau.2c00029
JACS Au 2022, 2, 1350−1358

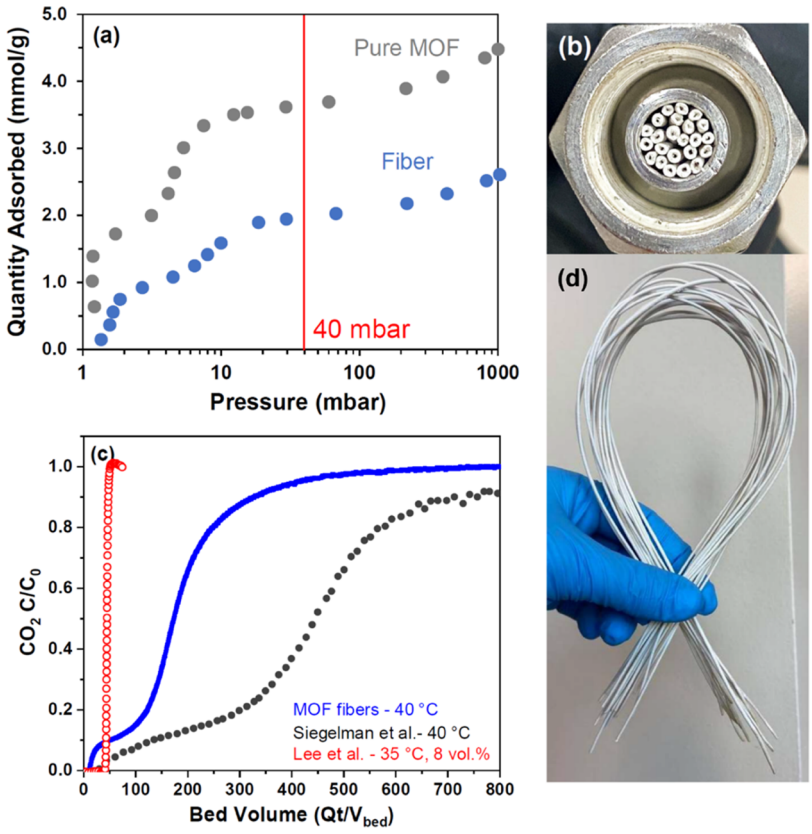

Figure 4. (a) CO_2 adsorption isotherm on pure 2-ampd-Mg_2(dobpdc) and 2-ampd-Mg_2(dobpdc)/PES hollow fiber sorbents at 40 °C, where MOF-based uptake is per g MOF and fiber-based uptake is per g fiber; (b) cross section of a module packed with 2-ampd-Mg2(dobpdc)/PES hollow fibers; and (c) CO_2 breakthrough curve on 2-ampd-Mg_2(dobpdc)/PES fibers (adsorption at 40 °C, 28 sccm, 4.5% CO_2/4.5% He/balance N_2; activation at 120 °C with 139 sccm Ar). The breakthrough is compared with the MOF powder in Siegelman et al.'s work[18] [reproduced with permission from ref 18. Copyright 2019 American Chemical Society] and diamine-Mg_2(dobpdc) fibers prepared by the post-treatment method in Lee et al.'s work.[32] (the breakthrough curve was converted from sorption time to bed volume) [reproduced with permission from ref 32. Copyright 2021 American Chemical Society]; (d) Fibers' flexibility.

versatility but also offering alternatives to engineering these materials based on application-driven purposes.

CO_2 Adsorption Performance on 2-ampd-Mg_2(dobpdc)/PES Hollow Fiber Sorbents

The CO_2 adsorption isotherm on 2-ampd-Mg_2(dobpdc)/PES hollow fiber sorbents at 40 °C is shown in Figure 4a. The isotherm at 40 °C exhibits the characteristic two-step adsorption due to the steric hindrance by 2-ampd on Mg_2(dobpdc). The CO_2 uptake at 40 mbar was approximately 2.0 mmol CO_2/g-fiber or 3.0 mmol CO_2/g-MOF. In Siegelman et al.'s work,[18] the CO_2 uptake on pure MOF powder at 40 mbar and 40 °C was about 3.4 mmol CO_2/g-sorb. Determined by the weight loss via TGA (Figure S18), the MOF loading is about 68 wt % in the total fiber. This shows that nearly 88% of the MOF initially in the dope was maintained after spinning into hollow fibers, indicating the scalable application of 2-ampd-Mg_2(dobpdc) hollow fiber sorbents.

The ultimate goal of this work is to utilize the hollow fiber sorbents in industrial applications. Therefore, breakthrough tests on 2-ampd-Mg_2(dobpdc)/PES hollow fibers for a simplified CO_2 capture demonstration were conducted. 2-ampd-Mg_2(dobpdc)/PES hollow fibers were aligned in a fixed-bed module with a void fraction of 0.35 (24 fibers). The cross section of the module and the fibers' flexibility are shown in Figure 4b,d. A simulated NGCC exhaust gas containing 4.5 mol % CO_2/N_2 with a He tracer was used as the feed gas. The experimental details are described in the Experimental Section. The breakthrough curves at 40°C are shown in Figure 4c, in which a similar "shock-wave-shock" breakthrough to the MOF particle fixed bed[18] was observed. Such a breakthrough trend is attributed to the step adsorption of the 2-ampd-Mg_2(dobpdc) in hollow fibers. The second step occurs at a CO_2 C/C_0 of approximately 0.1, which was at 0.4 vol % CO_2 concentration. As seen in the CO_2 isotherm at 40 °C in Figure 4a, the second step occurs at about 4 mbar, which is consistent with the breakthrough curve. The CO_2 uptake at 40 °C was 2.5 mmol CO_2/g-MOF, lower than the isotherm uptake at 40 mbar (i.e., 3.0 mmol CO_2/g-MOF), which matches the breakthrough results in Siegelman et al.'s work on the MOF particles in a fixed bed.[18] Compared to the fixed-bed particle sorbents, both "steps" of the breakthrough curve are sharper in the hollow fiber sorbent bed, which is indicative of more rapid mass transfer, as expected. In addition, the hollow fiber morphology has a benefit of a lower pressure drop compared to a conventional particle/pellet sorption bed, which was reported in our previous work.[19,42]

CONCLUSIONS

The high CO_2 uptake and water stability of 2-ampd-Mg_2(dobpdc) make it an appealing candidate for incorporation into hollow fiber composite contactors. The protocols we

https://doi.org/10.1021/jacsau.2c00029
JACS Au 2022, 2, 1350−1358

report for creating 2-ampd-Mg_2(dobpdc)/polymer hollow fiber sorbents via a direct spinning process are straightforward and scalable, eliminating complex steps in postspinning processes. Three polymers, CA, PES, and AO-PIM-1, are workable as polymer networks, while polyimides, such as Matrimid and Torlon, degrade in contact during the diamine infusion. Despite the lack of explicit study of kinetics, the results of the CO_2 adsorption isotherm and dynamic breakthrough experiments were consistent with those on MOF powder beds but with qualitatively faster adsorption kinetics and a lower pressure drop.

Nonetheless, there are some key limitations in our current work. First, this work is limited to CO_2 capture under dry conditions. As the humidity in postcombustion gas is nonnegligible, the influence of humidity on MOF hollow fiber sorbents is important and will be studied in our future work (although it is likely that the moisture will promote CO_2 adsorption, as it does on pure 2-ampd-Mg_2(dobpdc)[18]). Moreover, for a better utilization of MOF hollow fiber sorbents with heat integration through an RTSA process, a scalable one-step formation of a water-proof lumen layer in the bore side will be studied and investigated in subsequent work. Additionally, while energy analysis is beyond the scope of this work, the regeneration energy of an MOF hollow fiber is expected to be approximately 73 kJ/mol,[18] similar to a pure MOF due to the high loading of the MOF in the fiber.[43] With the study of heat integration and energy analysis, breakthrough modeling will be reported in future work focusing on utilizing MOF hollow fibers in a TSA process with thermal management, which has been studied in our previous work on hollow fiber sorbents using a TSA process.[44,45] In spite of these limitations, the simplified process described in this work is the first step toward utilizing novel and high-performance MOFs in industrial carbon capture processes.

■ ASSOCIATED CONTENT

Supporting Information

The Supporting Information is available free of charge at https://pubs.acs.org/doi/10.1021/jacsau.2c00029.

Illustration of "dry-jet, wet-quench" spinning process, dope compositions for syringe extrusion and spinning, synthesis of PIM-1 and AO-PIM-1, characterization experiments, CO_2 adsorption performance on different polymer-supported MOFs, CO_2 adsorption isobars on MOF fibers grafted with different amines, and polyimide degradation in amines (PDF)

■ AUTHOR INFORMATION

Corresponding Authors

Simon C. Weston − *Corporate Strategic Research, ExxonMobil Research and Engineering Company, Annandale, New Jersey 08801, United States;* orcid.org/0000-0002-7439-5055; Email: simon.c.weston@exxonmobil.com

Ryan P. Lively − *School of Chemical and Biomolecular Engineering, Georgia Institute of Technology, Atlanta, Georgia 30332, United States;* orcid.org/0000-0002-8039-4008; Email: ryan.lively@chbe.gatech.edu

William J. Koros − *School of Chemical and Biomolecular Engineering, Georgia Institute of Technology, Atlanta, Georgia 30332, United States;* orcid.org/0000-0001-5873-0899; Email: wjk@chbe.gatech.edu

Authors

Wenying Quan − *School of Chemical and Biomolecular Engineering, Georgia Institute of Technology, Atlanta, Georgia 30332, United States;* orcid.org/0000-0003-0409-0165

Hannah E. Holmes − *School of Chemical and Biomolecular Engineering, Georgia Institute of Technology, Atlanta, Georgia 30332, United States;* orcid.org/0000-0002-3199-1711

Fengyi Zhang − *School of Chemical and Biomolecular Engineering, Georgia Institute of Technology, Atlanta, Georgia 30332, United States;* orcid.org/0000-0002-2398-8176

Breanne L. Hamlett − *School of Chemistry & Biochemistry, Georgia Institute of Technology, Atlanta, Georgia 30332, United States*

M. G. Finn − *School of Chemistry & Biochemistry and School of Biological Sciences, Georgia Institute of Technology, Atlanta, Georgia 30332, United States;* orcid.org/0000-0001-8247-3108

Carter W. Abney − *Corporate Strategic Research, ExxonMobil Research and Engineering Company, Annandale, New Jersey 08801, United States*

Matthew T. Kapelewski − *Process Technology Department, ExxonMobil Research and Engineering Company, Annandale, New Jersey 08801, United States*

Complete contact information is available at: https://pubs.acs.org/10.1021/jacsau.2c00029

Notes

The authors declare no competing financial interest.

Georgia Tech Research Corporation and ExxonMobil Research and Engineering Company have applied for patents on some of the materials and processes discussed herein, on which W.Q., F.Z., M.G.F., C.W.A., M.T.K., R.P.L., W.J.K., and S.C.W. are included as inventors.

■ ACKNOWLEDGMENTS

This work was financially supported by ExxonMobil Research and Engineering Company. One of the polymers, poly(ether sulfone), was provided by Solvay. This work was performed in part at the Georgia Tech Institute for Electronics and Nanotechnology, a member of the National Nanotechnology Coordinated Infrastructure (NNCI), which is supported by the National Science Foundation (Grant ECCS-2025462).

■ REFERENCES

(1) Pachauri, R. K.; Allen, M. R.; Barros, V. R.; Broome, J.; Cramer, W.; Christ, R.; Church, J. A.; Clarke, L.; Dahe, Q.; Dasgupta, P. *Climate Change 2014: Synthesis Report. Contribution of Working Groups I, II and III to the Fifth Assessment Report of the Intergovernmental Panel on Climate Change*; IPCC, 2014.

(2) IEA *Global Energy Review 2021*; IEA: Paris, 2021.

(3) Rochelle, G. T. Amine Scrubbing for CO_2 Capture. *Science* **2009**, *325*, 1652−1654.

(4) Yu, C.-H.; Huang, C.-H.; Tan, C.-S. A Review of CO_2 Capture by Absorption and Adsorption. *Aerosol Air Qual. Res.* **2012**, *12*, 745−769.

(5) Grande, C. A.; Ribeiro, R. P. L.; Oliveira, E. L. G.; Rodrigues, A. E. Electric Swing Adsorption as Emerging CO_2 Capture Technique. *Energy Procedia* **2009**, *1*, 1219−1225.

(6) Grande, C.; Rodrigues, A. Electric Swing Adsorption for CO_2 Removal from Flue Gases. *Int. J. Greenhouse Gas Control* **2008**, *2*, 194−202.
(7) Clausse, M.; Merel, J.; Meunier, F. Numerical Parametric Study on CO_2 Capture by Indirect Thermal Swing Adsorption. *Int. J. Greenhouse Gas Control* **2011**, *5*, 1206−1213.
(8) Merel, J.; Clausse, M.; Meunier, F. Experimental Investigation on CO_2 Post-Combustion Capture by Indirect Thermal Swing Adsorption Using 13X and 5A Zeolites. *Ind. Eng. Chem. Res.* **2008**, *47*, 209−215.
(9) Song, C. Global Challenges and Strategies for Control, Conversion and Utilization of CO_2 for Sustainable Development Involving Energy, Catalysis, Adsorption and Chemical Processing. *Catal. Today* **2006**, *115*, 2−32.
(10) Chang, F.-Y.; Chao, K.-J.; Cheng, H.-H.; Tan, C.-S. Adsorption of CO_2 onto Amine-Grafted Mesoporous Silicas. *Sep. Purif. Technol.* **2009**, *70*, 87−95.
(11) Belmabkhout, Y.; Serna-Guerrero, R.; Sayari, A. Adsorption of CO_2-Containing Gas Mixtures over Amine-Bearing Pore-Expanded MCM-41 Silica- Application for Gas Purification. *Ind. Eng. Chem. Res.* **2010**, *49*, 359−365.
(12) Abu-Zahra, M. R. M.; Schneiders, L. H. J.; Niederer, J. P. M.; Feron, P. H. M.; Versteeg, G. F. CO_2 Capture from Power Plants: Part I. A Parametric Study of the Technical Performance Based on Monoethanolamine. *Int. J. Greenhouse Gas Control* **2007**, *1*, 37−46.
(13) Boutin, A.; Couck, S.; Coudert, F.-X.; Serra-Crespo, P.; Gascon, J.; Kapteijn, F.; Fuchs, A. H.; Denayer, J. F. M. Thermodynamic Analysis of the Breathing of Amino-Functionalized MIL-53(Al) upon CO_2 Adsorption. *Microporous Mesoporous Mater.* **2011**, *140*, 108−113.
(14) Abid, H. R.; Rada, Z. H.; Shang, J.; Wang, S. Synthesis, Characterization, and CO_2 Adsorption of Three Metal-Organic Frameworks (MOFs): MIL-53, MIL-96, and Amino-MIL-53. *Polyhedron* **2016**, *120*, 103−111.
(15) Choi, S.; Watanabe, T.; Bae, T. H.; Sholl, D. S.; Jones, C. W. Modification of the Mg/DOBDC MOF with Amines to Enhance CO_2 Adsorption from Ultradilute Gases. *J. Phys. Chem. B* **2012**, *3*, 1136−1141.
(16) McDonald, T. M.; Lee, W. R.; Mason, J. A.; Wiers, B. M.; Hong, C. S.; Long, J. R. Capture of Carbon Dioxide from Air and Flue Gas in the Alkylamine-Appended Metal-Organic Framework mmen-Mg2(dobpdc). *J. Am. Chem. Soc.* **2012**, *134*, 7056−7065.
(17) McDonald, T. M.; Mason, J. A.; Kong, X.; Bloch, E. D.; Gygi, D.; Dani, A.; Crocella, V.; Giordanino, F.; Odoh, S. O.; Drisdell, W. S.; Vlaisavljevich, B.; Dzubak, A. L.; Poloni, R.; Schnell, S. K.; Planas, N.; Lee, K.; Pascal, T.; Wan, L. F.; Prendergast, D.; Neaton, J. B.; Smit, B.; Kortright, J. B.; Gagliardi, L.; Bordiga, S.; Reimer, J. A.; Long, J. R. Cooperative Insertion of CO_2 in Diamine-Appended Metal-Organic Frameworks. *Nature* **2015**, *519*, 303−308.
(18) Siegelman, R. L.; Milner, P. J.; Forse, A. C.; Lee, J. H.; Colwell, K. A.; Neaton, J. B.; Reimer, J. A.; Weston, S. C.; Long, J. R. Water Enables Efficient CO_2 Capture from Natural Gas Flue Emissions in an Oxidation-Resistant Diamine-Appended Metal-Organic Framework. *J. Am. Chem. Soc.* **2019**, *141*, 13171−13186.
(19) Hughes, R.; Kotamreddy, G.; Ostace, A.; Bhattacharyya, D.; Siegelman, R. L.; Parker, S. T.; Didas, S. A.; Long, J. R.; Omell, B.; Matuszewski, M. Isotherm, Kinetic, Process Modeling, and Techno-Economic Analysis of a Diamine-Appended Metal−Organic Framework for CO_2 Capture Using Fixed Bed Contactors. *Energy Fuels* **2021**, *35*, 6040−6055.
(20) Lively, R. P.; Chance, R. R.; Kelley, B. T.; Deckman, H. W.; Drese, J. H.; Jones, C. W.; Koros, W. J. Hollow Fiber Adsorbents for CO_2 Removal from Flue Gas. *Ind. Eng. Chem. Res.* **2009**, *48*, 7314−7323.
(21) Lively, R. P.; Leta, D. P.; DeRites, B. A.; Chance, R. R.; Koros, W. J. Hollow Fiber Adsorbents for CO_2 Capture-Kinetic Sorption Performance. *Chem. Eng. J.* **2011**, *171*, 810−819.
(22) Labreche, Y.; Lively, R. P.; Rezaei, F.; Chen, G.; Jones, C. W.; Koros, W. J. Post-Spinning Infusion of Poly(ethyleneimine) into Polymer/Silica Hollow Fiber Sorbents for Carbon Dioxide Capture. *Chem. Eng. J.* **2013**, *221*, 166−175.
(23) Rezaei, F.; Lively, R. P.; Labreche, Y.; Chen, G.; Fan, Y.; Koros, W. J.; Jones, C. W. Aminosilane-Grafted Polymer/Silica Hollow Fiber Adsorbents for CO_2 Capture from Flue Gas. *ACS Appl. Mater. Interfaces* **2013**, *5*, 3921−3931.
(24) Fan, Y.; Labreche, Y.; Lively, R. P.; Jones, C. W.; Koros, W. J. Dynamic CO_2 Adsorption Performance of Internally Cooled Silica-Supported Poly(ethylenimine) Hollow Fiber Sorbents. *AIChE J.* **2014**, *60*, 3878−3887.
(25) Labreche, Y.; Fan, Y.; Rezaei, F.; Lively, R. P.; Jones, C. W.; Koros, W. J. Poly(amide-imide)/Silica Supported PEI Hollow Fiber Sorbents for Postcombustion CO_2 Capture by RTSA. *ACS Appl. Mater. Interfaces* **2014**, *6*, 19336−19346.
(26) Fan, Y.; Kalyanaraman, J.; Labreche, Y.; Rezaei, F.; Lively, R. P.; Realff, M. J.; Koros, W. J.; Jones, C. W.; Kawajiri, Y. CO_2 Sorption Performance of Composite Polymer/Aminosilica Hollow Fiber Sorbents: An Experimental and Modeling Study. *Ind. Eng. Chem. Res.* **2015**, *54*, 1783−1795.
(27) Labreche, Y.; Fan, Y.; Lively, R. P.; Jones, C. W.; Koros, W. J. Direct Dual Layer Spinning of Aminosilica/Torlon Hollow Fiber Sorbents with a Lumen Layer for CO_2 Separation by Rapid Temperature Swing Adsorption. *J. Appl. Polym. Sci.* **2015**, *132*, 41845−41854.
(28) DeWitt, S. J. A. *Thermally Modulated Fiber Sorbents for Rapidly Cycled Vacuum-Pressure Swing Adsorption of Post-Combustion Flue Gas*; Georgia Institute of Technology, 2020.
(29) Chen, G.; Koros, W. J.; Jones, C. W. Hybrid Polymer/UiO-66(Zr) and Polymer/NaY Fiber Sorbents for Mercaptan Removal from Natural Gas. *ACS Appl. Mater. Interfaces* **2016**, *8*, 9700−9709.
(30) Pimentel, B. R.; Fultz, A. W.; Presnell, K. V.; Lively, R. P. Synthesis of Water-Sensitive Metal−Organic Frameworks within Fiber Sorbent Modules. *Ind. Eng. Chem. Res.* **2017**, *56*, 5070−5077.
(31) Darunte, L. A.; Terada, Y.; Murdock, C. R.; Walton, K. S.; Sholl, D. S.; Jones, C. W. Monolith-Supported Amine-Functionalized Mg2(dobpdc) Adsorbents for CO_2 Capture. *ACS Appl. Mater. Interfaces* **2017**, *9*, 17042−17050.
(32) Lee, Y. H.; Kwon, Y.; Kim, C.; Hwang, Y. E.; Choi, M.; Park, Y.; Jamal, A.; Koh, D. Y. Controlled Synthesis of Metal-Organic Frameworks in Scalable Open-Porous Contactor for Maximizing Carbon Capture Efficiency. *JACS Au* **2021**, *1*, 1198−1207.
(33) Weston, S. C.; Abney, C. W.; Falkowski, J. M.; Ivashko, A. C. US Application No. 17/601,610, 2021.
(34) Abney, C. W.; Seo, J. J.; Quan, W.; Koros, W. J.; Lively, R. P.; Peters, A. W.; Ivashko, A. C.; Kapelewski, M. T.; Weston, S. C. US Application No. 63/282,796, 2021.
(35) Jue, M. L.; Breedveld, V.; Lively, R. P. Defect-Free PIM-1 Hollow Fiber Membranes. *J. Membr. Sci.* **2017**, *530*, 33−41.
(36) Jue, M. L.; McKay, C. S.; McCool, B. A.; Finn, M. G.; Lively, R. P. Effect of Nonsolvent Treatments on the Microstructure of PIM-1. *Macromolecules* **2015**, *48*, 5780−5790.
(37) Yi, S.; Ghanem, B.; Liu, Y.; Pinnau, I.; Koros, W. J. Ultraselective Glassy Polymer Membranes with Unprecedented Performance for Energy-Efficient Sour Gas Separation. *Sci. Adv.* **2019**, *5*, 5495−5505.
(38) Zuluaga, S.; Fuentes-Fernandez, E. M. A.; Tan, K.; Xu, F.; Li, J.; Chabal, Y. J.; Thonhauser, T. Understanding and Controlling Water Stability of MOF-74. *J. Mater. Chem. A* **2016**, *4*, 5176−5183.
(39) Vitillo, J. G.; Bordiga, S. Increasing the Stability of Mg_2(dobpdc) Metal−Organic Framework in Air Through Solvent Removal. *Mater. Chem. Front.* **2017**, *1*, 444−448.
(40) Li, F. S.; Qiu, W.; Lively, R. P.; Lee, J. S.; Rownaghi, A. A.; Koros, W. J. Polyethyleneimine-Functionalized Polyamide Imide (Torlon) Hollow-Fiber Sorbents for Post-Combustion CO_2 Capture. *ChemSusChem* **2013**, *6*, 1216−1223.
(41) Kappert, E. J.; Raaijmakers, M. J. T.; Tempelman, K.; Cuperus, F. P.; Ogieglo, W.; Benes, N. E. Swelling of 9 Polymers Commonly Employed for Solvent-Resistant Nanofiltration Membranes: A Comprehensive Dataset. *J. Membr. Sci.* **2019**, *569*, 177−199.

https://doi.org/10.1021/jacsau.2c00029
JACS Au 2022, 2, 1350−1358

(42) Lively, R. P.; Leta, D. P.; DeRites, B. A.; Chance, R. R.; Koros, W. J. Hollow Fiber Adsorbents for CO_2 Capture: Kinetic Sorption Performance. *Chem. Eng. J.* **2011**, *171*, 801−810.
(43) Kalyanaraman, J.; Fan, Y.; Lively, R. P.; Koros, W. J.; Jones, C. W.; Realff, M. J.; Kawajiri, Y. Modeling and Experimental Validation of Carbon Dioxide Sorption on Hollow Fibers Loaded with Silica-Supported Poly(ethylenimine). *Chem. Eng. J.* **2015**, *259*, 737−751.
(44) Lively, R. P.; Chance, R. R.; Mysona, J. A.; Babu, V. P.; Deckman, H. W.; Leta, D. P.; Thomann, H.; Koros, W. J. CO_2 Sorption and Desorption Performance of Thermally Cycled Hollow Fiber Sorbents. *Int. J. Greenhouse Gas Control* **2012**, *10*, 285−294.
(45) Rezaei, F.; Subramanian, S.; Kalyanaraman, J.; Lively, R. P.; Kawajiri, Y.; Realff, M. J. Modeling of Rapid Temperature Swing Adsorption Using Hollow Fiber Sorbents. *Chem. Eng. Sci.* **2014**, *113*, 62−76.

https://doi.org/10.1021/jacsau.2c00029
JACS Au 2022, 2, 1350−1358